AGN

FEASIBILITY DETERMINATION OF A NUCLEAR THERMIONIC SPACE POWER PLANT

Contract No. AF 33(657)-8977
Project No. 8173
Task No. 817305-10

QUARTERLY TECHNICAL PROGRESS REPORT

For Period

1 November 1962 through 31 January 1963

AN-973

June 1963

GENERAL TIRE

NOTICE

"The work covered by this report was accomplished under Air Force Contract AF 33(657)-8977, but this report is being published and distributed prior to Air Force review. The publication of this report, therefore, does not constitute approval by the Air Force of the findings or conclusions contained herein. It is published for the exchange and stimulation of ideas."

FEASIBILITY DETERMINATION

OF A

NUCLEAR THERMIONIC SPACE POWER PLANT

Quarterly Technical Progress Report

For Period

1 February 1963 through 30 April 1963

Report AN-973

Contract No. AF 33(657)-8977
Project No. 8173
Task No. 817305-10

Reviewed by: K E Buck
K. E. Buck, Project Engineer

Reviewed and Approved by: K. P. Johnson
K. P. Johnson
Manager, Space Power Department

Aerojet-General NUCLEONICS
A SUBSIDIARY OF AEROJET-GENERAL CORPORATION
SAN RAMON, CALIFORNIA

CONTENTS

ILLUSTRATIONS

I. OBJECTIVE

The work described in this report is aimed at demonstrating the feasibility of the Nuclear Thermionic Radiator Space Power System. It is a continuation of work initiated on Contract AF 33(616)-8119. The specific objectives of the current program are:

1) To demonstrate operation of at least three thermionic converters in series array, using heat from a liquid metal loop to heat the cathodes

2) To demonstrate 1000 hours of thermionic operation using liquid metal heating

II. INTRODUCTION

The thermionic radiator system will utilize a nuclear heat source to produce electrical power in space. A combined thermionic converter-radiator unit is coupled with a high temperature, liquid metal cooled, fast reactor heat source; coolant is circulated directly through the radiator and back to the reactor in a single loop. Cylindrical thermionic converters filled with cesium vapor encircle the tube walls of the radiator. Emitters (on the radiator tubes) are heated by conduction through the tube wall. Collectors concentric to the cathode dissipate waste heat directly to space through attached fins.

One aspect of the feasibility of the thermionic radiator system is to be demonstrated by operating three generators with heat from a single liquid metal loop. The generators, to be electrically connected in series, are of a type being developed by RCA under Contract AF 33(657)-8005. The converters are cylindrical and will be mounted on a columbium alloy tube, using an electrically insulating thermal bond. The liquid metal loop on which these converters will be mounted will be fabricated from the same columbium alloy. Lithium will be circulated in the loop by natural convection. The entire system will be placed in a vacuum chamber to protect the refractory metals from oxidation.

In addition to this experimental work, a thermal transport analysis is being conducted to aid in selection of loop test parameters and to allow overall system characteristics to be investigated. The current status of the work is as follows:

1) The thermal transport analysis, except for details of radiator configuration, has been completed.

2) The liquid metal loop is partly constructed. Delivery of the thermionic generators has been delayed because of fabrication difficulties associated with the electrically insulating thermal bond between the generator and the liquid metal tubing.

III. TECHNICAL PROGRESS

Technical work on this program has been divided into the following three tasks:

Task 2 - Liquid Metal Tubing - Converter Bond

Task 3 - Thermal Transport Analysis

Task 4 - Series Unit Loop Test

Task 2 was completed prior to the period covered in this report. Technical progress on Tasks 3 and 4 is discussed below.

A. TASK 3 - THERMAL TRANSPORT ANALYSIS

During this quarter, attention has been directed to degradation of converter performance resulting from series operation, the effect of emitter temperature variation on converter performance, and calculation of micrometeoroid armor requirements. These separate efforts are described below.

1. Effect of Emitter Temperature on Converter Performance

The effect on power density of series-connecting converters operating at different emitter temperatures for the range 1300 to 1175^{o}C was found to result from connecting converters electrically in series over this temperature region. Non-optimum performance can result from connecting converters electrically in parallel when the emitter temperatures differ, unless output voltages are carefully matched. The effect on power density of a linear emitter temperature variation in an individual converter was calculated for a temperature drop of up to 40^{o}C.

Power and efficiency can be lost when thermionic converters are series-connected, if units are not perfectly matched with respect to the current produced at optimum operating conditions. Mismatching can occur either from variation in fabrication and processing of the particular converters, or from variation in operating temperature; only this second consideration is discussed here. Since, in the thermionic radiator approach, heat is extracted from a liquid metal stream to supply converters with thermal energy, the cathode temperature will decrease along the length of a series of converters as well as along each individual converter, and some degradation in output will result from this temperature differential between series-connected units.

a. Series Connection

To evaluate the effect of series-connecting thermionic converters, representative current-voltage performance characteristics must be obtained. The shortage of experimental data at the low temperature operating range of interest (about 1200°C) severely handicaps this analysis. Although it was intended to collect and compare all published data for the molybdenum cathode-anode system to determine characteristic voltage-current performance, lack of reproducibility obtained by various investigators testing converters under operating conditions stated to be identical, made it impossible to establish such information; it was, therefore, necessary to use data from a single source. Calculations are based on the findings of Baum and Jensen (General Electric Company) shown in Figure 1. The results of extrapolating this information to lower temperatures over a limited I-V region are given in Figure 2. Low voltage arc mode operating characteristics for a range in emitter temperature of 1175 to 1300°C are summarized in Figure 3.

The series-connection of converters demands that the current be the same in each device. As evident from Figure 3, this condition can be satisfied (about 7 amps/cm^2) throughout the specified temperature range without deviating significantly from the maximum power condition for each operating temperature; fortuitously, peak power is obtained at almost the same current density. At high cesium pressure, variations in converter performance attributable to temperature differences are minimized

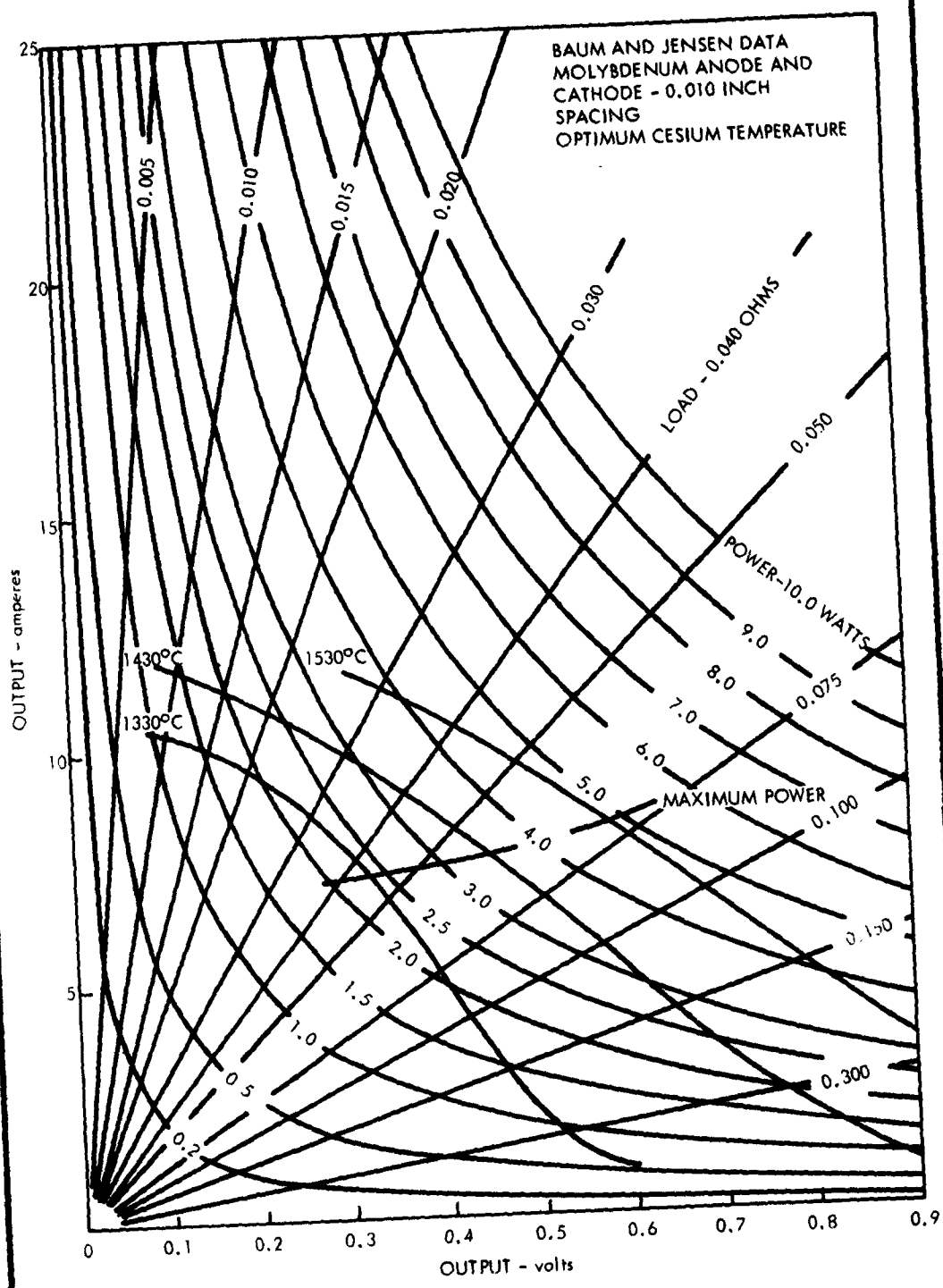

FIGURE 1. THERMIONIC CONVERTER OPERATING CHARACTERISTICS

170-65-22252

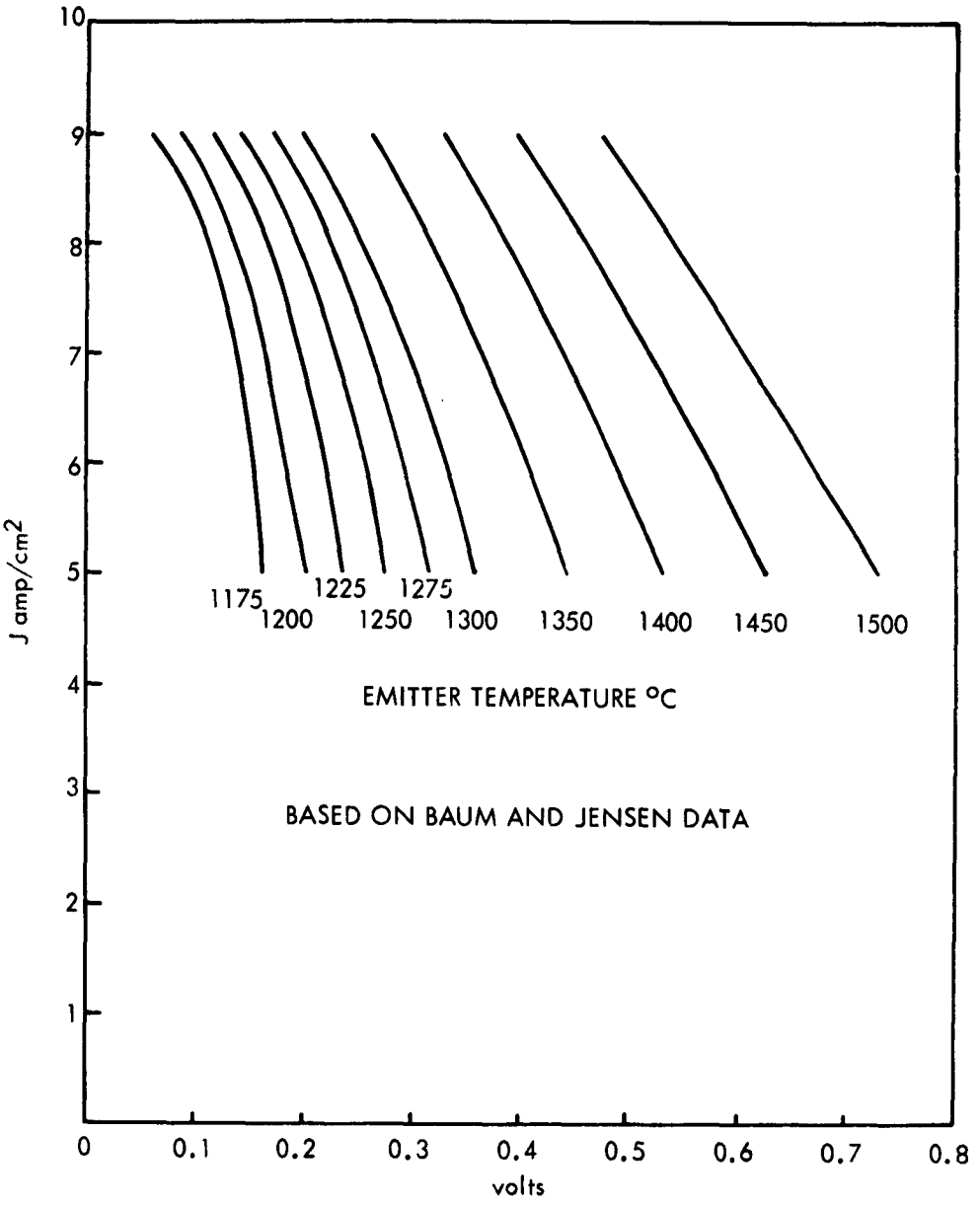

FIGURE 2. EXTRAPOLATED CURRENT - VOLTAGE CURVES

17.0-63-2253

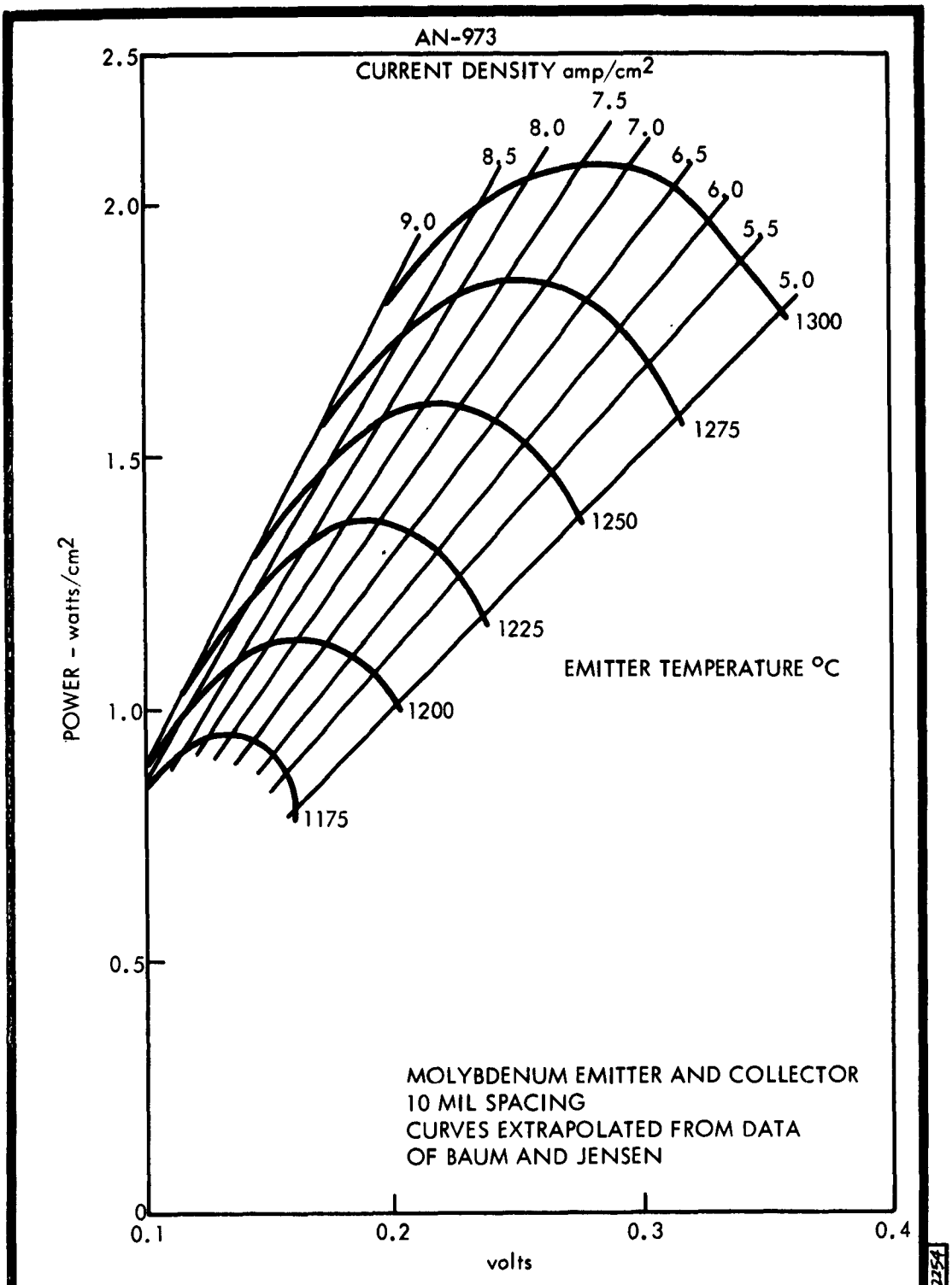

FIGURE 3. LOW VOLTAGE ARC MODE OPERATING CHARACTERISTICS

by a self-compensating effect. A temperature decrease lowers the emitter work function due to increased cesium coverage; this tends to increase electron emission and compensate for the loss caused by lower emitter temperature. This compensation is very nearly complete for the case considered. As a result of the lowered emitter work function, less output voltage is obtained, and the net effect of a temperature decrease is less power.

For the operating region considered, no significant degradation in converter performance due to non-optimum operation is expected as a result of series-connecting converters operating at different temperatures. Near peak performance can be obtained from each converter; however, the power output from each device will obviously decrease as the emitter temperature decreases. The effect of emitter temperature on peak power density is shown in Figure 4. Because converter power density is very nearly linear over this temperature range, the average power density of a number of series connected devices corresponds to that of the average emitter operating temperature, since the deviation from optimum conditions at each converter is negligible.

b. Parallel Connection

In the preceeding analysis, it was found that near optimum performance can be obtained from converters connected in series, since peak power is obtained at almost the same converter current density over the operating temperature range considered (1175 to 1300^{o}C). This is apparent from the converter operating characteristics shown in Figure 3. It is equally apparent that sizeable divergence from optimum conditions can be incurred by operating converters in parallel where the voltage across each device is the same. For example, if the voltage corresponds to maximum power for an emitter temperature of 1300^{o}C (0.29 volts), a converter connected in parallel operating with an emitter temperature of 1175^{o}C would provide negligible power output. This serious consequence is emphasized by considering the parallel connection of two individual converters operating at significantly different temperatures. Power loss from converters operating in parallel can be completely eliminated by series-connecting a sufficient number of low temperature converters to match the optimum voltage output of the high temperature converters. In the thermionic

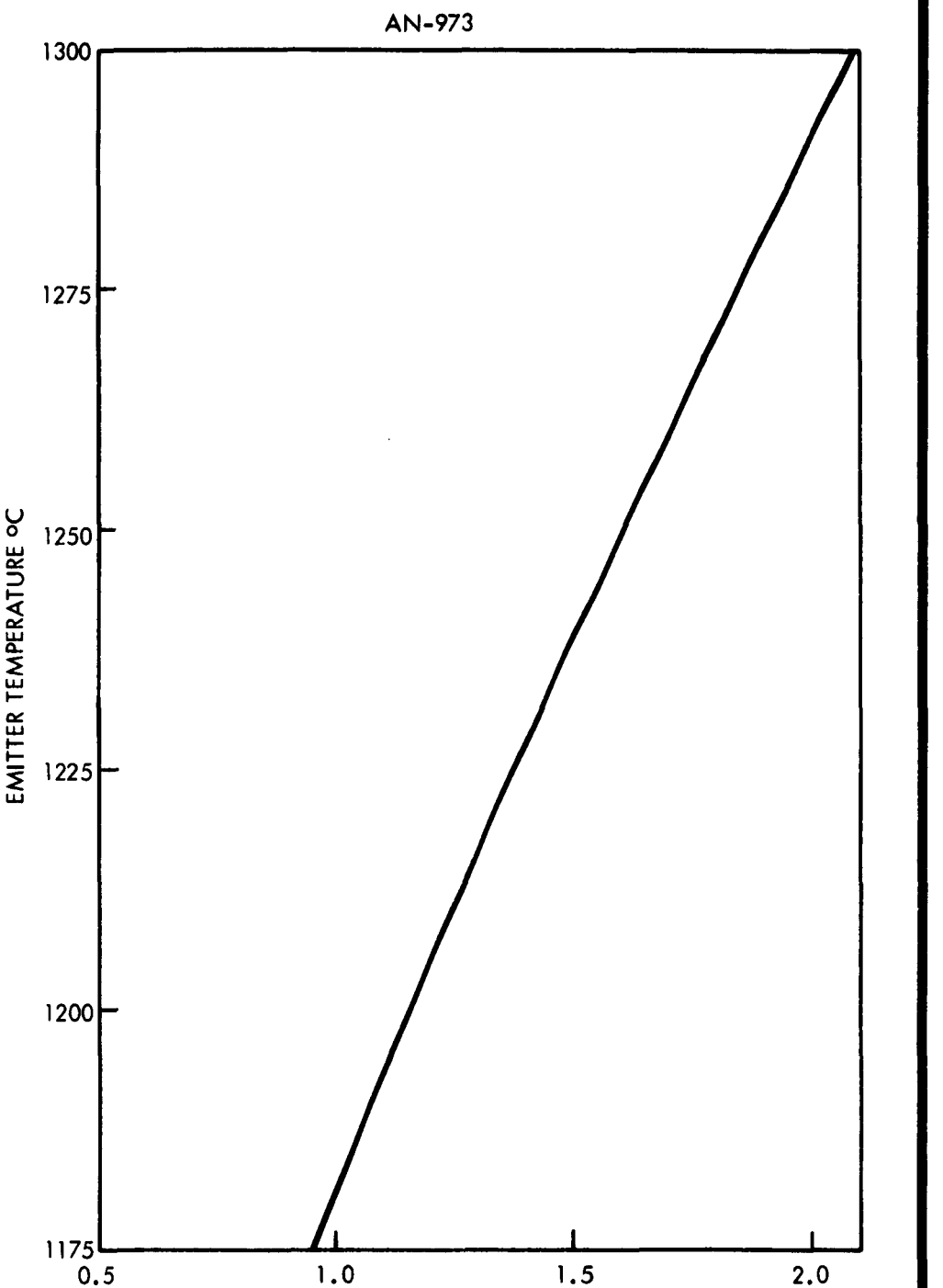

FIGURE 4. MAXIMUM POWER DENSITY VERSUS EMITTER TEMPERATURE

radiator system, a number of series-connected converters are joined in parallel to similar radiator segments, each operating over the same total temperature difference. Since temperatures are identical, no power loss will result from parallel connections, if each converter can be fabricated to provide identical operating characteristics. But if large numbers of series connected converters show significant variation, it may be necessary to increase flexibility during assembly so that the proper number of converters can be series-connected in each radiator segment to assure matched total output voltage.

c. Temperature Variation in Individual Converter

Thus far, the analysis is based on an individual converter operating at a uniform emitter temperature; however, since heat is continuously removed from the liquid metal stream, the emitter temperature will vary along the length of each converter. The observed converter output should be equivalent to that of a large number of diodes connected electrically in parallel, but operating at different emitter temperatures, as illustrated in Figure 5.

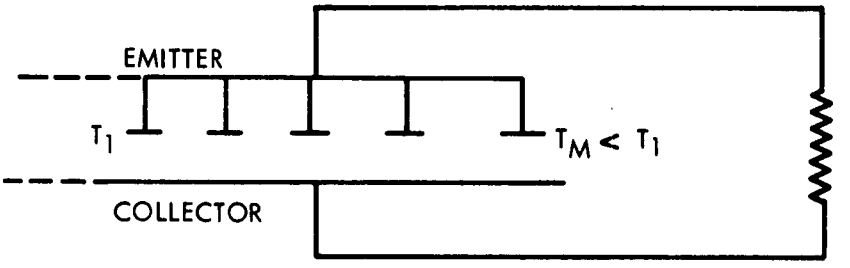

FIGURE 5. EQUIVALENT CIRCUIT FOR CONVERTER WITH EMITTER TEMPERATURE VARIATION

From the preceding considerations, it is apparent that, if the temperature variation is large, low temperature emitter regions of the converter may be very ineffective and that, consequently, the temperature difference along

an individual converter must be minimized. Since the total temperature drop along a single converter will depend on the overall radiator configuration, but in no case will exceed 40°C, the power loss associated with an emitter temperature variation can be estimated as follows. A typical motive diagram for high cesium pressure thermionic converter operation (Figure 6) will be used as a model for the analysis.

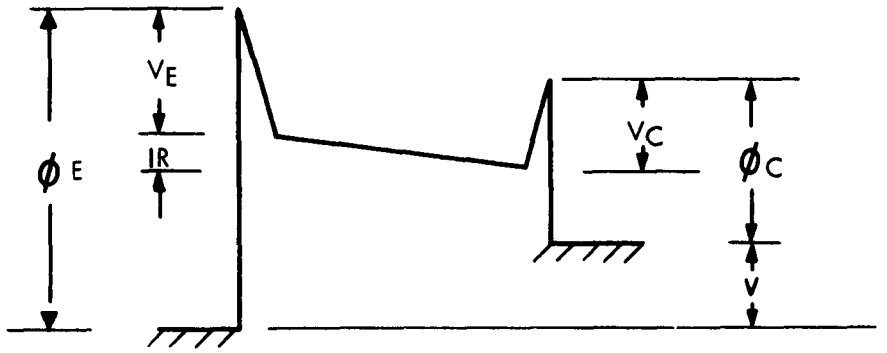

FIGURE 6. TYPICAL THERMIONIC CONVERTER MOTIVE DIAGRAM (HIGH CESIUM PRESSURE OPERATION)

The net current flowing through the converter can be expressed at the emitter side in terms of the potential V_E of the emitter sheath and the random electron current, I_e, in the plasma:

$$I = I_s - I_e e^{-e V_E/k T_e} \qquad (1)$$

The same current can be expressed at the collector side in terms of the potential V_c of the collector sheath and the random electron current in the plasma:*

*E. N. Carabateas, S. D. Pezaris, and G. N. Hatsopoulos, "Intepretation of Experimental Characteristics of Cesium Thermionic Converters," J. Appl. Phys., 32, 352 (1961).

$$I = I_e \, e^{-e\, V_c/k\, T_e} \,, \qquad (2)$$

where I = net current,

I_e = random electron current,

I_s = emitter saturation current,

V_E = emitter sheath potential,

V_c = collector sheath potential, and

T_e = temperature of electrons.

The assumption was made that the plasma is uniform, which implies that the electron concentration, electron temperature and, therefore, random electron current are the same at the two edges of the plasma next to the emitter and collector. The ion current was neglected on both the emitter and collector side, since it is generally small compared to the net electron current. From Equation (2),

$$I_e = Ie^{\,e\, V_c/k\, T_e} \,,$$

and by eliminating I_e in Equation (1),

$$I = I_s - Ie^{\,-e\,(V_E - V_c)/k\, T_e} \;;$$

solving for I, then,

$$I = I_s/1 + e^{-e\,(V_E - V_c)/k\, T_e} \,. \qquad (3)$$

Assuming that the collector and emitter sheath potentials and electron temperature are constant for constant output voltage over the small emitter temperature range considered,

$$1 + e^{-e\,(V_E - V_c)/k\, T_e} = e^K = \text{constant},$$

the net electron current density, J, can be expressed as:

$$J = A\, T^2 \, e^{-e\,(\phi_E + K)/k\, T} \,, \qquad (4)$$

where A = Richardson constant,

T = emitter temperature, and

ϕ_E = emitter work function.

The observed total output current from the converter is then the sum of the currents from each of the small diodes connected in parallel along the emitter surface. The average current density, J, for a cylindrical emitter can therefore be expressed as

$$\bar{J} = \frac{1}{L} \int_0^L J(X)\, dx, \tag{5}$$

where $J(x) = A\, T^2(X)\, \exp\left[- \frac{e\, \phi}{k\, T(X)} \right]$,

and $\phi = \phi_E + K$ = constant.

The emitter work function, ϕ_E, is assumed to be constant over the small temperature range considered, which is only strictly valid for vacuum converters. This represents a worst case solution, then, inasmuch as the emitter work function decreases as the temperature decreases, and would tend to reduce the calculated emission loss. For a linear emitter temperature distribution,

$$T(X) = T_o\, (1 - \alpha X),$$

the integral equation can be expressed as:

$$\bar{J} = \frac{A\, T_o^{\,2}}{\alpha L} \int_1^{\gamma_o} \frac{1}{\gamma^4} \exp\left(- \frac{e\, \phi\, \gamma}{k\, T_o} \right) d\gamma \ , \tag{6}$$

where $\gamma = 1/1 - \alpha X$,

$\gamma_o = T_1/T_L$,

T_o = maximum emitter temperature,

T_L = minimum emitter temperature, and

L = converter length.

The solution to Equation (6) is:

$$\bar{J} = \frac{A\,T_o^{\,3}}{(T_o - T_L)} \left[E_4\left(\frac{e\,\phi}{k\,T_o}\right) - \left(\frac{T_L}{T_o}\right)^3 E_4\left(\frac{e\,\phi}{k\,T_L}\right) \right] \qquad (7)$$

where $E_4(X) = X^3 \int_X^{\infty - t} \frac{e}{t^4}\, dt$.

Equation (7) was solved for $T_o = 1200^{\circ}C$ and $0 \leq \left(T_o - T_L\right) \leq 40^{\circ}C$, assuming

$$J\ (1200^{\circ}C) = 7.0\ \text{amps/cm}^2;$$

therefore, $\phi_E + K = \phi = 2.21$ for $A = 120\ \text{amp/cm}^2\ {}^{\circ}K^2$.

These results are illustrated in Figure 7. Since the output voltage is constant across the converter, Figure 7 also depicts the effect of temperature drop on converter power density.

2. Micrometeoroid Shielding Calculations

Problems associated with the micrometeoroid shielding of the thermionic radiator system were briefly reviewed, including the latest estimates of the micrometeoroid flux distribution and comparisons of various penetration models. Equations describing the required armor thicknesses were formulated. The review and derivations appear as Appendix I. The results of this analysis can be expressed in terms of two equations for

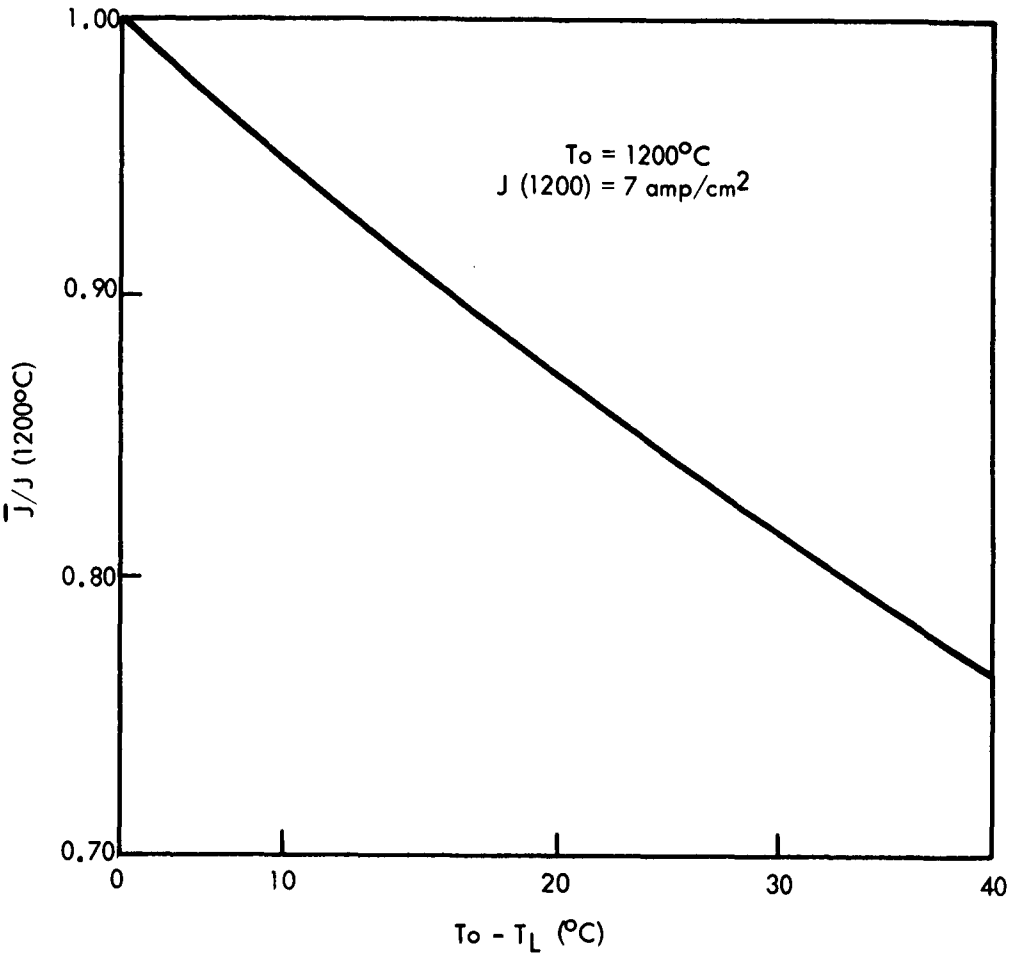

FIGURE 7. EFFECT OF LINEAR EMITTER TEMPERATURE DROP ON CONVERTER CURRENT DENSITY

17.0-67-2258

the equivalent armor thickness. The protection afforded the liquid metal tubing by converter materials and armor is given by:

$$t_{equiv} = \left(\frac{E_{tube}}{E_{armor}}\right)^{0.334} \left(\frac{\rho_{tube}}{\rho_{armor}}\right)^{0.166} t_{tube}$$

$$+ \left(\frac{E_{conv}}{E_{armor}}\right)^{0.334} \left(\frac{\rho_{conv}}{\rho_{armor}}\right)^{0.166} t_{conv} + t_{external\ armor}$$

where E = Young's Modulus of material indicated,

ρ = density of material indicated, and

t = thickness of material indicated.

The armor thickness required for a given radiator area, assuming a specified mission time and the probability that no punctures will occur, is given by:

$$t = \left[\frac{5.5}{E_a^{0.334}\,\rho_a^{0.166}}\right]\left[\frac{\tau}{-\ln P(o)}\right]^{0.249}\left[N\left(A_i + 2\pi L\,\frac{t_{equiv}}{30.48}\right)\right]^{0.249},$$

where E_a = Youngs Modulus of armor,

ρ_a = density of armor,

τ = mission time,

$P(o)$ = probability of no critical damage,

A_i = inside surface area of radiator tube

L = length of radiator tube, and

N = Number of radiator tubes.

Using these relations, armor calculations were made for the following parameters.

Armor Parameters	
Material	Beryllium
Density	1.85 gm/cc
Young's Modulus	37×10^6 psi
Tube Parameters	
Material	Cb-1Zr
Density	8.56 gm/cc
Young's Modulus	14.4×10^6 psi
Wall Thickness	0.030 in. = 0.076 cm
Converter Parameters	
Material	Molybdenum
Density	10.2 gm/cc
Young's Modulus	42×10^6 psi
Wall Thickness (cathode + anode)	0.040 in. = 0.102 cm
Penetration Parameters	
Mission Time	10^4 hrs = 417 days
Probability of Non-puncture	95%

Substitution of these parameters into Equations (1) and (2) yields the following results:

$$t_{equiv} = \left(\frac{14.4}{37}\right)^{0.334} \left(\frac{8.56}{1.85}\right)^{0.166} 0.076 +$$

$$+ \left(\frac{42}{37}\right)^{0.334} \left(\frac{10.2}{1.85}\right)^{0.166} 0.102 + t_a$$

$$= 0.0715 + 0.141 + t_a = 0.213 + t_a \qquad (3)$$

$$t_{equiv} = \left[\frac{5.5}{(37 \times 10^6)^{0.334} (1.85)^{0.166}}\right]\left[\frac{417}{-\ln 0.95}\right]^{0.249}\left[N\ (A_i + 0.206\ L\ t_{eq})\right]^{0.249}$$

$$t_{eq} = \left[0.01485\right]\left[9.4\right]\left[N(A_i + 0.206\ L\ t_{eq})\right]^{0.249}$$

$$= 0.1395 \left[N \left(A_i + 0.206 \, L \, t_{eq} \right) \right]^{0.249} \qquad (4)$$

Combining Equations (3) and (4) and simplifying gives:

$$(NA_i) + 0.206 \, (NL_i) \, \delta = 2730 \, \delta^{4.02} \, , \qquad (5)$$

where t_a (in) $= \frac{\delta - 0.213}{2.54}$. If t_a is negative, then no armor is required beyond that provided by the tube and converter. The solution for Equation (5) for a selected range of variables is shown in Figure 8.

Table 1 provides an example of the application of this curbe for the following conditions:

Power level = 300 kw(e) net output
= 345 kw(e) output at radiator

Emitter diameter = 0.8 inch

Tube length required for seals = 5% emitter length

TABLE 1

MICROMETEOROID SHIELDING REQUIREMENTS

Emmitter power density - w/cm^2	1.0	0.5	2.0
Total emitter area - ft^2	372	248	186
Total wetted area - ft^2	342	228	171
Total tube length - ft	1870	1250	933
Shielding required - inch	0.19	0.16	0.14

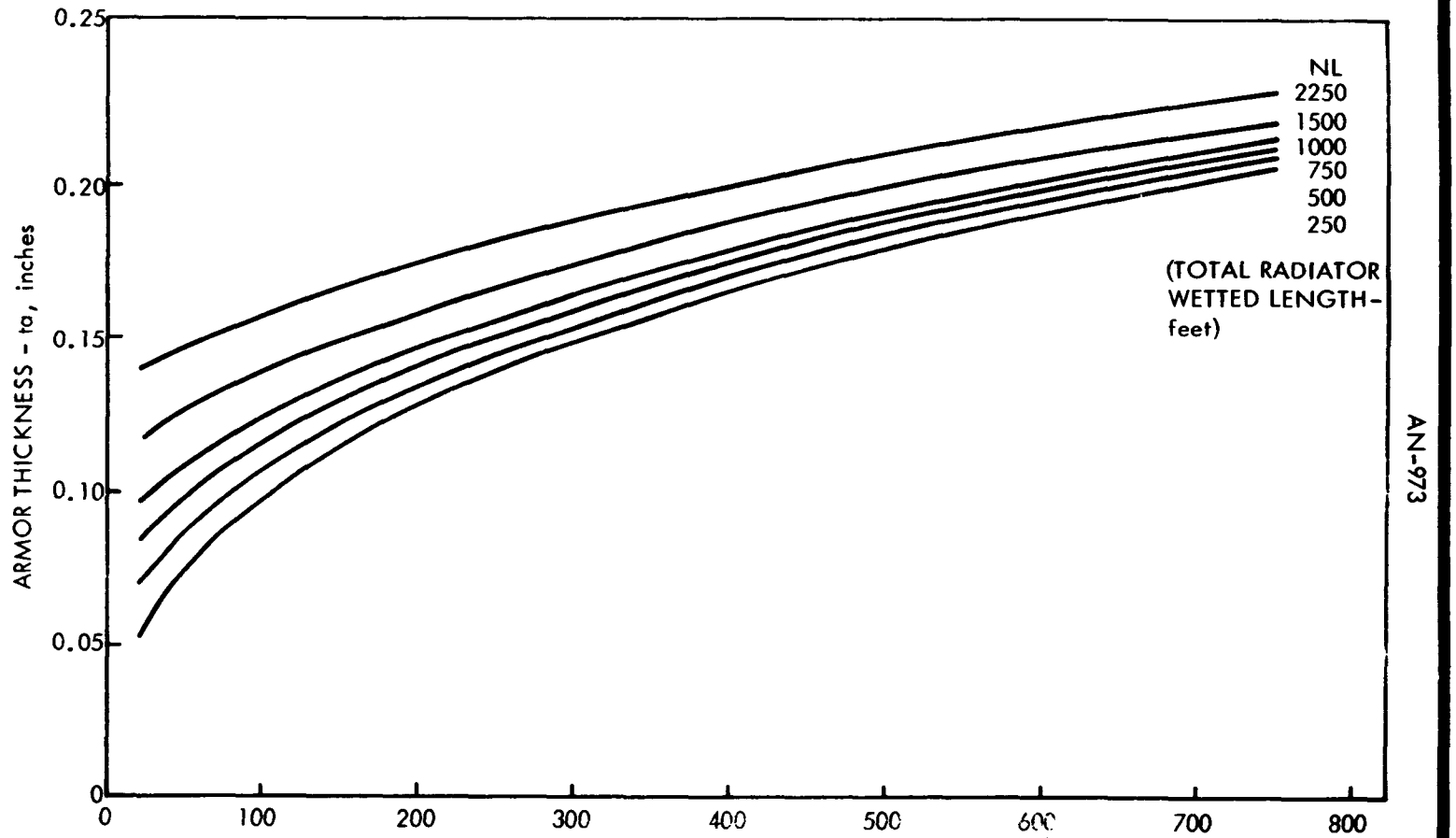

FIGURE 8. ARMOR THICKNESS VERSUS RADIATOR GEOMETRY - τ = 10,000 hours, B (o) = 0.95

B. TASK 4 - SERIES UNIT LOOP TEST

The natural convection loop described in the previous quarterly report has been partly fabricated. The general loop configuration is shown in Figure 9, and the construction status of major loop components is described below:

1. Main Heater

All molybdenum and columbium heater components have been fabricated. The main molybdenum bar was machined from sintered molybdenum; the studs and nuts were machined from arc-cast molybdenum. The weight of the molybdenum bar will be transmitted to the support stand by a spring-loaded support rod, and spring tension will be adjusted so that the columbium loop will be unloaded at operating temperature.

2. Heat Sink

Both heat sink units have been completely fabricated. All braze joints, except those between the copper caps and the stainless steel tubes, were made with vacuum brazing techniques. Braze alloys and temperatures are summarized in Table 2. The stainless steel tubes will be brazed to the copper heads by means of a tungsten/inert gas brazing technique applied in an inert atmosphere chamber. Successful test brazes have been made on a heat sink mockup, using a silver-copper-lithium alloy.

TABLE 2

HEAT SINK BRAZE SUMMARY

Joining Materials	Braze Alloy	Braze Temperature
Columbium-Molybdenum	Gold-Palladium	2200°F
Molybdenum-Copper	Gold-Nickel	1750°F
Copper-Copper	Silver-Copper	1450°F

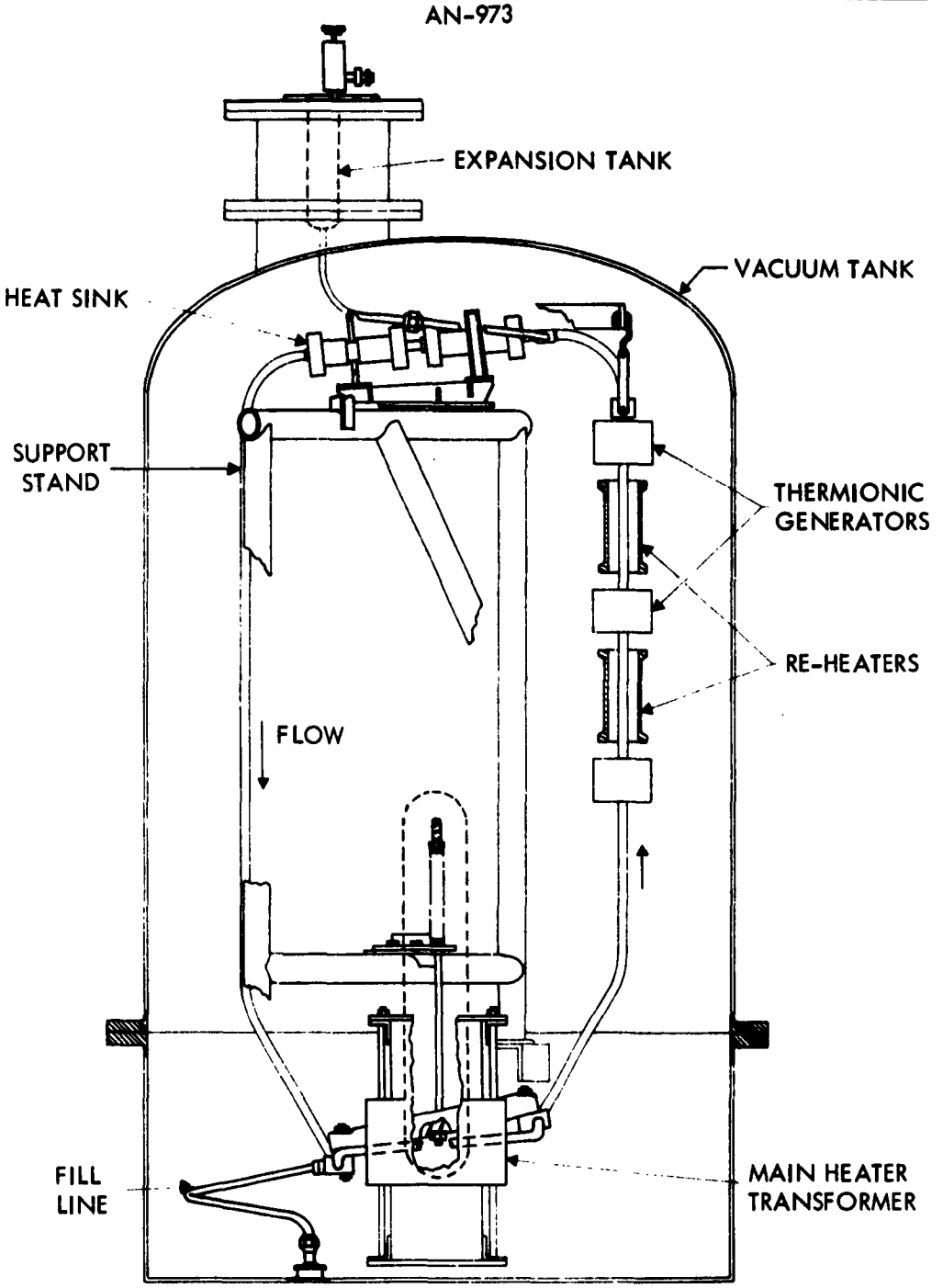

FIGURE 9. NATURAL CONVECTION LOOP CONFIGURATION

3. Support Stand

The stainless steel support stand on which the loop will be mounted has been fabricated. The brackets which will support the loop at various points have also been constructed and include:

1) A rigid support for the upper heat sink

2) A vertical support for the lower heat sink

3) The spring-loaded support for the molybdenum heater bar

4) The thermionic assembly support

This last support is attached to the loop at the top of the thermionic assembly. The support beam is counter-balanced to compensate for the weight of the three thermionic generators, thus eliminating the bending load on the section of the loop between the thermionic generators and the heat sink.

4. Thermionic Generators

The thermionic generators for this loop are being fabricated by RCA under subcontract to AGN, and are identical to those developed by RCA for ASD under Contract AF 33(657)-8005. The general specifications of the converter are:

1) The converter emitter will be molybdenum.

2) The center mounting tubing will be columbium-1% zirconium.

3) The entire converter assembly will be capable of withstanding a temperature of 500°C without deleterious effect.

4) The converter will employ a concentric cylindrical configuration, as follows:

Emitter OD	0.85 to 1.050 inches
Emitter active length	2.0 to 2.5 inches
Emitter area	40 cm^2
Converter length (excluding tubing)	4.25 inches (maximum)

Figure 10 is a drawing of the complete converter assembly.

Four converters under construction at RCA were scheduled for delivery to AGN by 11 April 1963. Just prior to shipment, however, a vacuum leak-check revealed small leaks in the inner columbium tube. Although the cracks in no way affected converter performance, they would permit liquid metal to escape, thus rendering them useless for their intended application. Fabrication was suspended and the design is being re-examined.

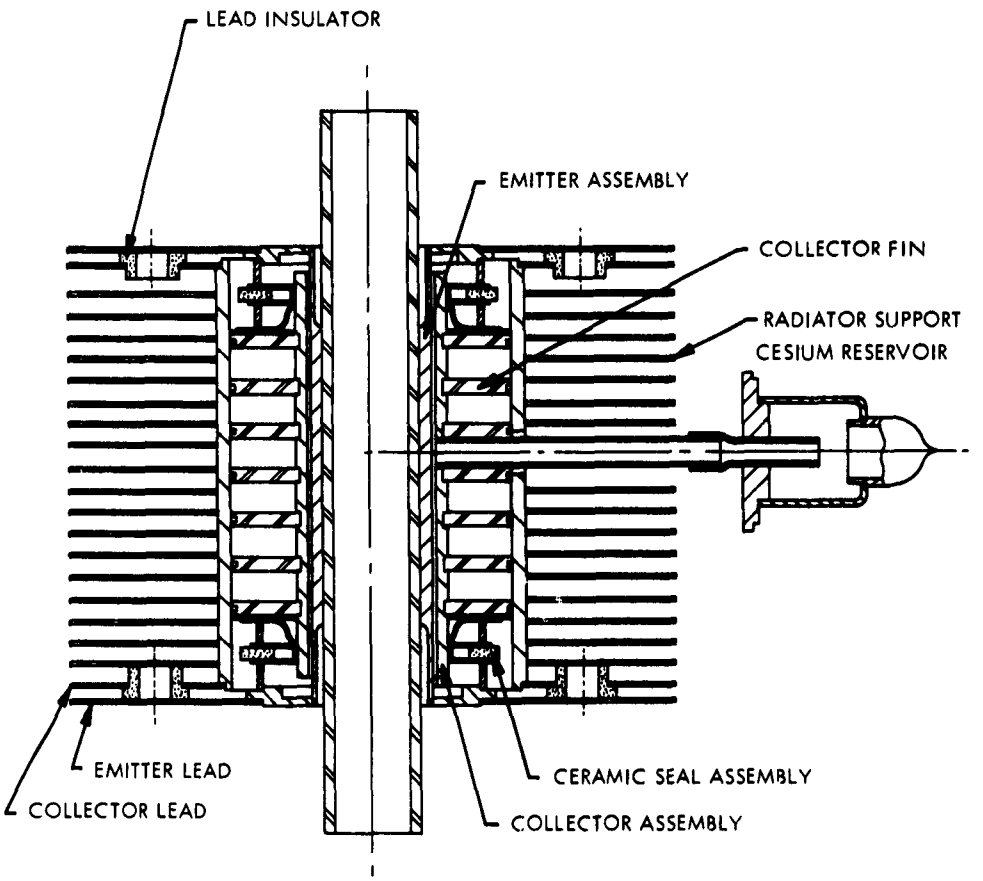

FIGURE 10. THERMIONIC CONVERTER ASSEMBLY DRAWING

170-63-2261

IV. FUTURE PLANS

Delivery of the modified thermionic converters is not expected until 31 August 1963. Loop fabrication and construction of auxiliary components will proceed at a reduced level of effort during the next three months. After the converters have been delivered, loop fabrication will be completed and testing will begin.

APPENDIX I

MICROMETEOROID SHIELDING REVIEW AND DERIVATIONS

I. OBJECTIVE

This appendix reviews various micrometeoroid shielding problems. The most recent estimates of flux distribution, comparisons of penetration models, and equations from which the required armor thickness can be derived are presented. A generalized set of curves, giving the required armor thickness as a function of radiator size for an assumed mission time, survival probabilities, and materials selection in a typical thermionic radiator system, is included.

II. DISCUSSION

The design of a space power system necessitates consideration of many environmental effects. One of the most disconcerting conditions confronting the radiator designer is that posed by the micrometeoroid flux in space. Vulnerable radiator areas must be shielded to reduce the probability of damage or puncture and consequent loss of fluid inventory, and this invariably increases radiator weight. Micrometeoroid problems are discussed below and design procedures for attaining the desired protection are derived, using the latest flux distributions and penetration correlations.

A. ORIGIN AND COMPOSITION

It is currently believed that 90% of the meteoroids are of cometary origin and that the remaining 10% are fragments of astroids. The density of the cometary meteoroids has been estimated to vary from 0.05 gm/cc for very porous particles to 3.5 gm/cc. The astroidal meteoroid particle densities are estimated to vary between 3.5 gm/cc and 8 gm/cc. The most recent reliable estimates place the average meteoroid density at 0.6 gm/cc.

B. METEOROID FLUX DENSITY

Various estimates have been made for the meteoroid flux in the vicinity of the earth, the most recent resulting from the Harvard. Trailblazer experiments performed in 1962. This information is plotted in Figure A-1, together with comparable data from other observers. The data may be expressed in the form of the following equation:

$$F_{>} = \alpha\, m^{-\beta},$$

where, according to the data,

$\alpha = 1.01 \times 10^{-10}$,

$\beta = 1.34$, and

m = meteoroid mass in grams.

Observations indicate that the meteoroid flux is anistropic, that is, a function of direction in space. It can be seen from the radar observations given in Figure A-2 that the apparent flux is greatest on the side of the earth facing the earth's motion, and that most of the particles are traveling in the same direction as the earth. Figure A-3 shows that most of the meteoric particles have trajectories at small angles to the plane of the ecliptic. Based on overall anistropricity, the radiator vulnerability can be reduced by a controlled orientation.

The velocity limits of particles observed from the earth lie between 11 and 73 km/sec. The lower limit is the minimum theoretical velocity that a particle would have if it fell from infinity to the earth under the action of the earth's gravitational force. The upper limit is based on the assumption that the earth runs into particles which move in retrograde orbit around the sun. Figure A-4 gives the velocity distribution of shower and sporadic meteors. The average meteoric velocity is estimated to be approximately 30 km/sec.

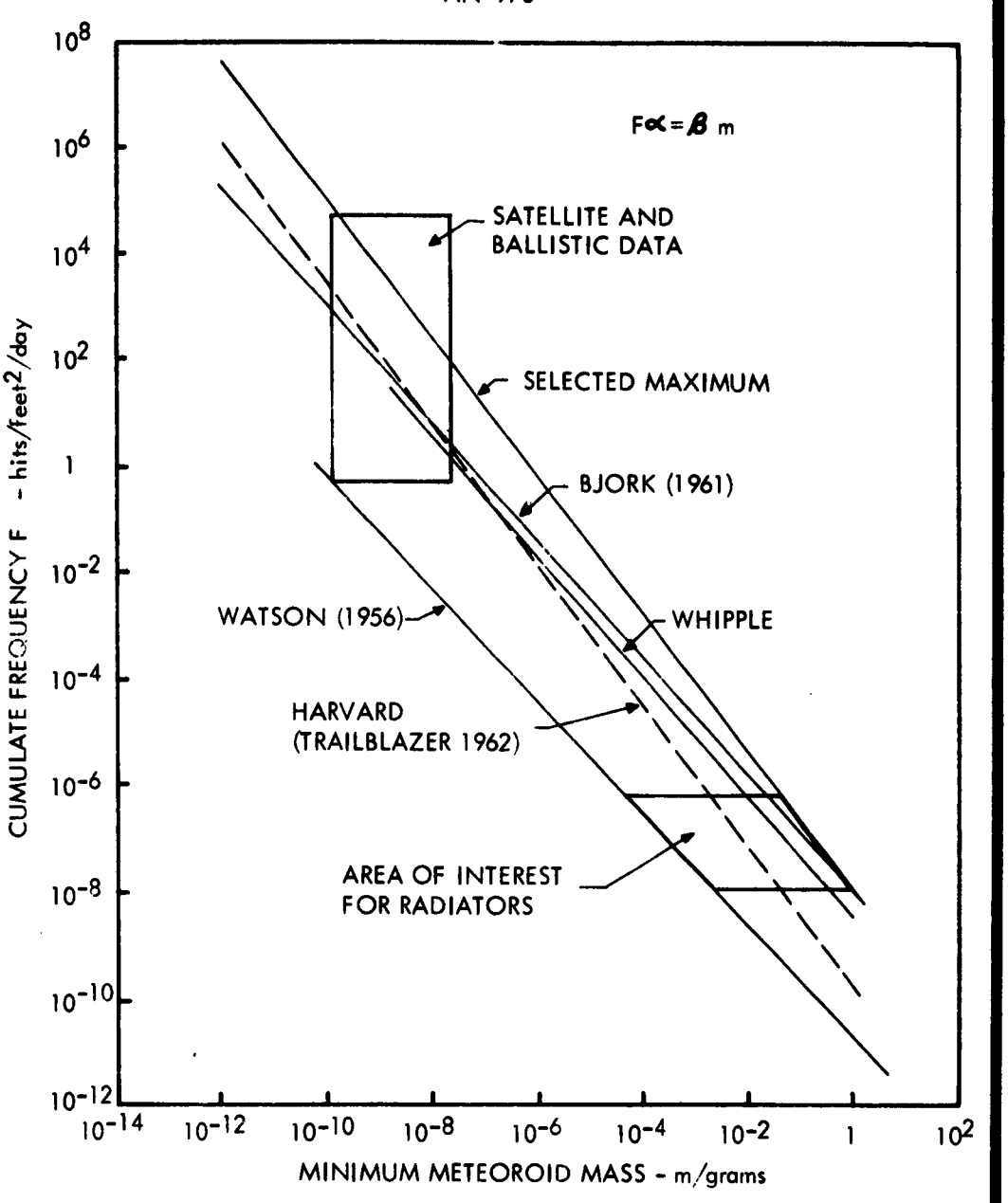

FIGURE A-1. METEOROID MASS - FREQUENCY DISTRIBUTION (FROM ARS 2543-62)

17.0-63-2245

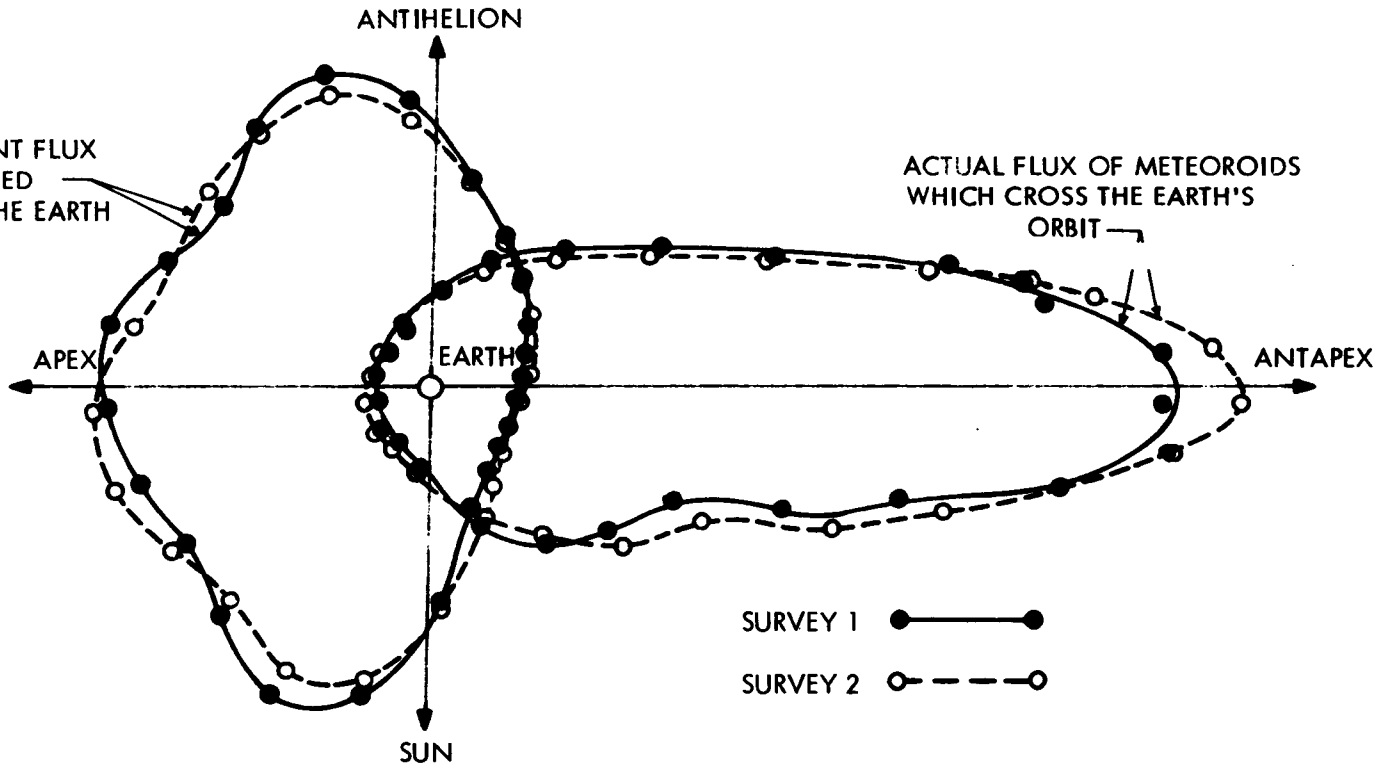

FIGURE A-2. POLAR DIAGRAM IN PLANE OF EARTH'S ORBIT SHOWING APPARENT NUMBER OF METEOR RADIANTS PER UNIT ANGLE PER SECOND (FROM NASA TN-D-1493)

17.0-63-2246

AN-973

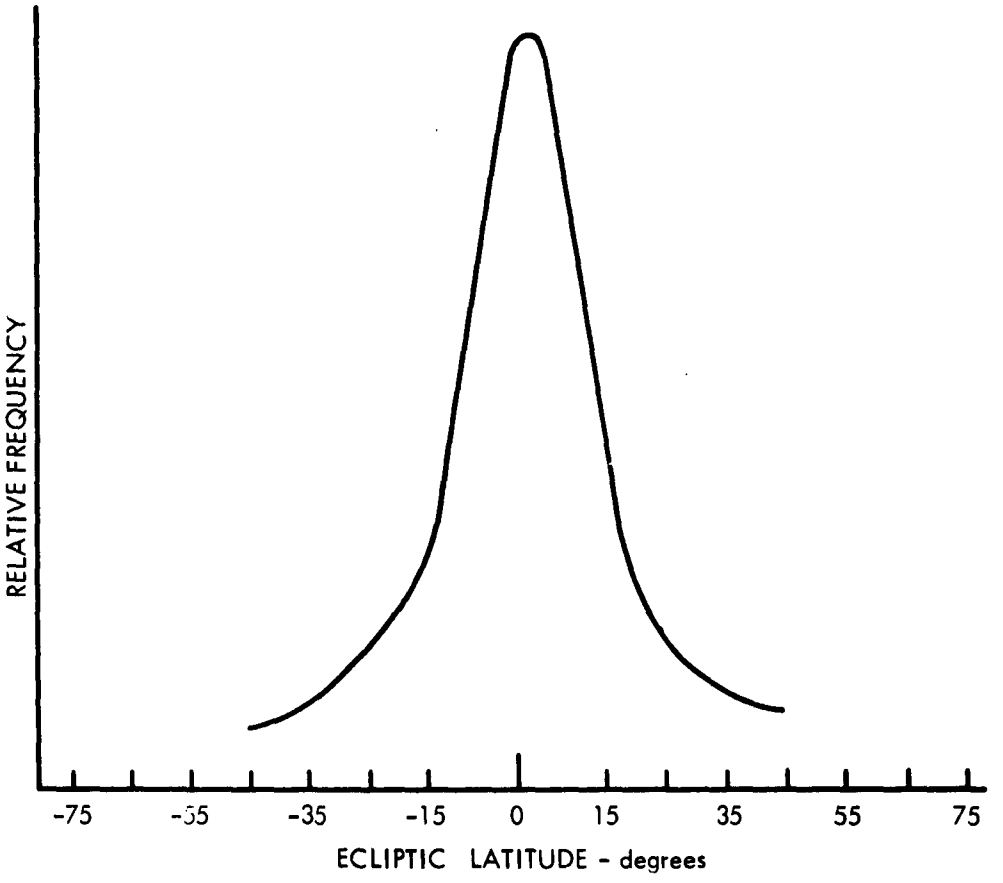

FIGURE A-3. DISTRIBUTION OF METEOR FLUX ABOUT THE PLANE OF THE ECLIPTIC (FROM NASA TN-D-1493)

17.0-63-2247

17.0-63-2248

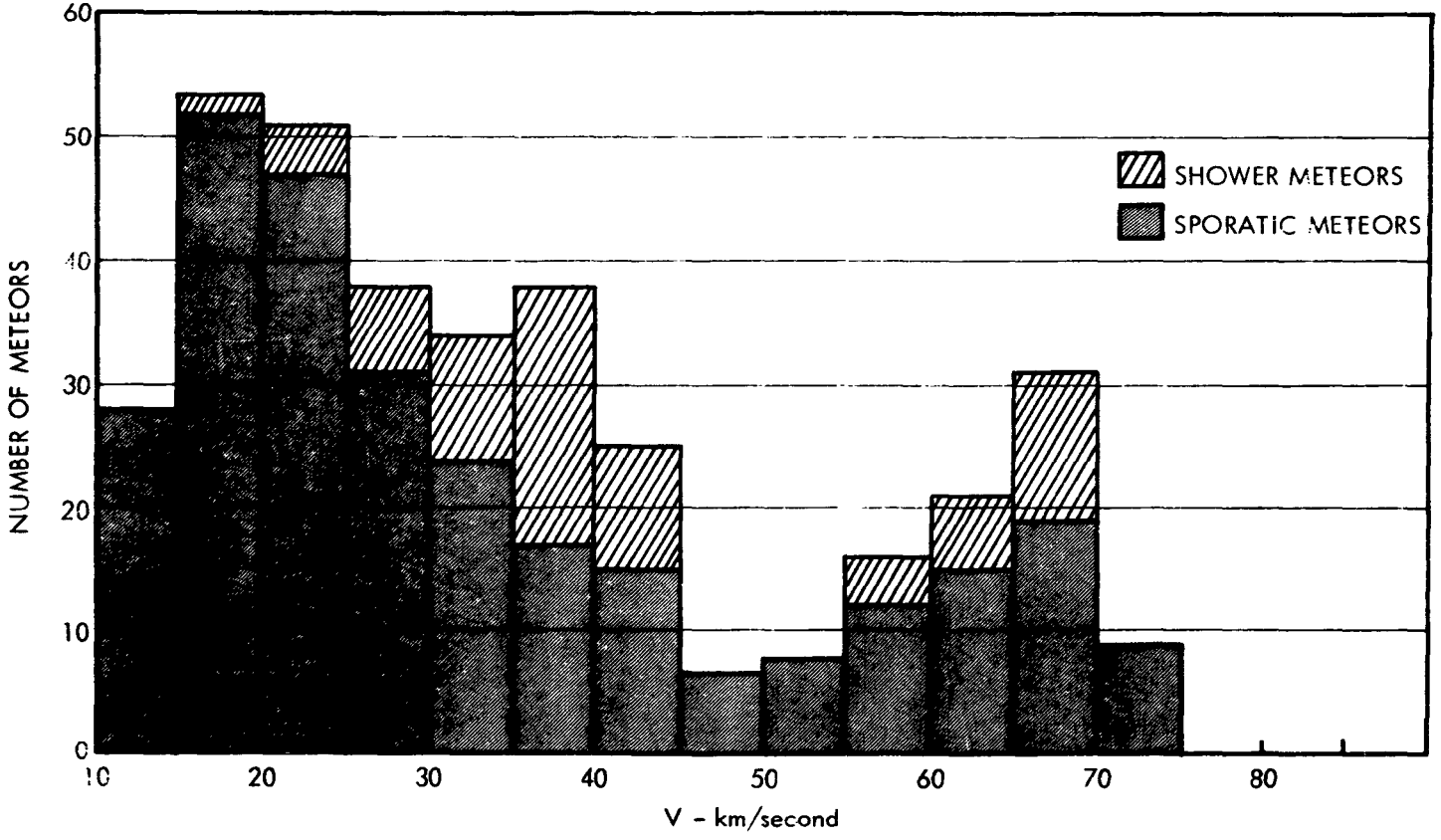

FIGURE A-4. METEORIC VELOCITY DISTRIBUTION (FROM NASA TN-D-1493)

AN-973

C. HYPERVELOCITY IMPACT

The hypervelocity impact process is complex and not yet well understood, expecially in the velocity ranges of interest to the radiator designer. To date, several different impact regions have been established (Figure A-5). In the undeformed projectile region, the penetration depth varies approximacely as the 4/3 power of projectile velocity, while in the transitional region, penetration does not seem to vary strongly with velocity. In the fluid flow region, the target material behaves as a fluid. The pertinent or meteoroid impact region is uncertain because no experimental data are available. On the basis of data accrued with currently attainable velocities, many investigators have obtained results for penetration of infinite targets which can be expressed by:

$$P_{\infty} = \gamma\, d \left(\frac{\rho_p}{\rho_T}\right)^{\phi} \left(\frac{\overline{v}}{c}\right)^{\theta} .$$

The penetration theories derived theoretically or from limted experimental data are compared in Figure A-6. Most investigators found the penetration to vary as the 2/3 power of velocity, although Bjork obtained an exponent of 1/3. The exponent θ is 1/3 for a momentum-dependent cratering process and 2/3 for a kinetic energy-dependent process. The penetration calculations use 1/2 for θ.

D. PROTECTION METHODS

Micrometeoroid structural damage can be generally categorized as follows, and each category requires a different degree of protection.

1) Perforation - results in loss of working fluid, cesium, etc.

2) Intrusion - energy of incident particle transmitted to fluid, possibly causing damage by shock wave propogation at local or distant points.

3) Surface Damage - reduces structural integrity, emissive coating effectiveness.

4) Functional Damage - introduces deformations which could interfere with the components functions.

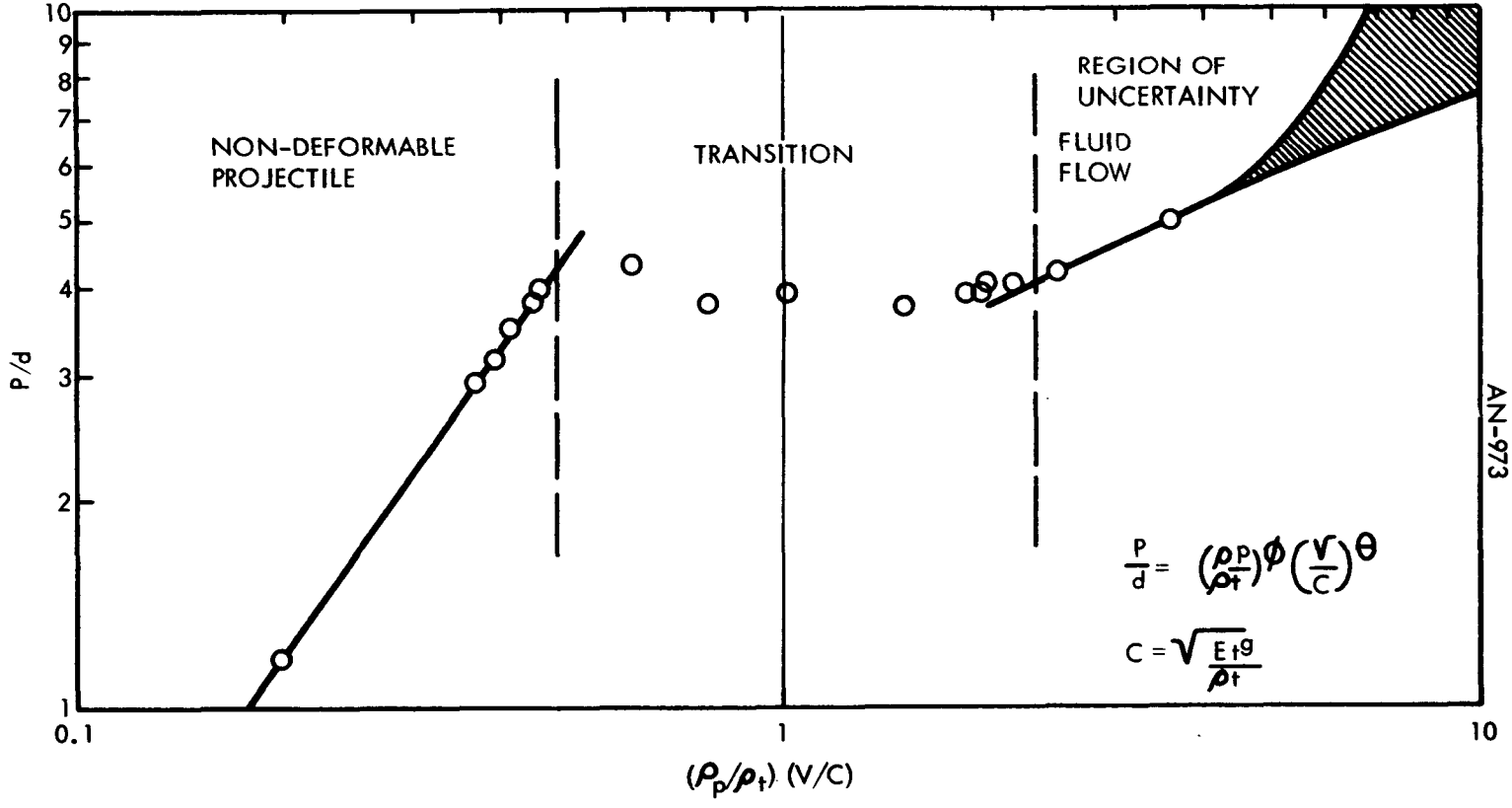

FIGURE A-5. PENETRATION VERSUS DENSITY RATIO IMPACT MACHINE NUMBER (FROM ARS 2543-62)

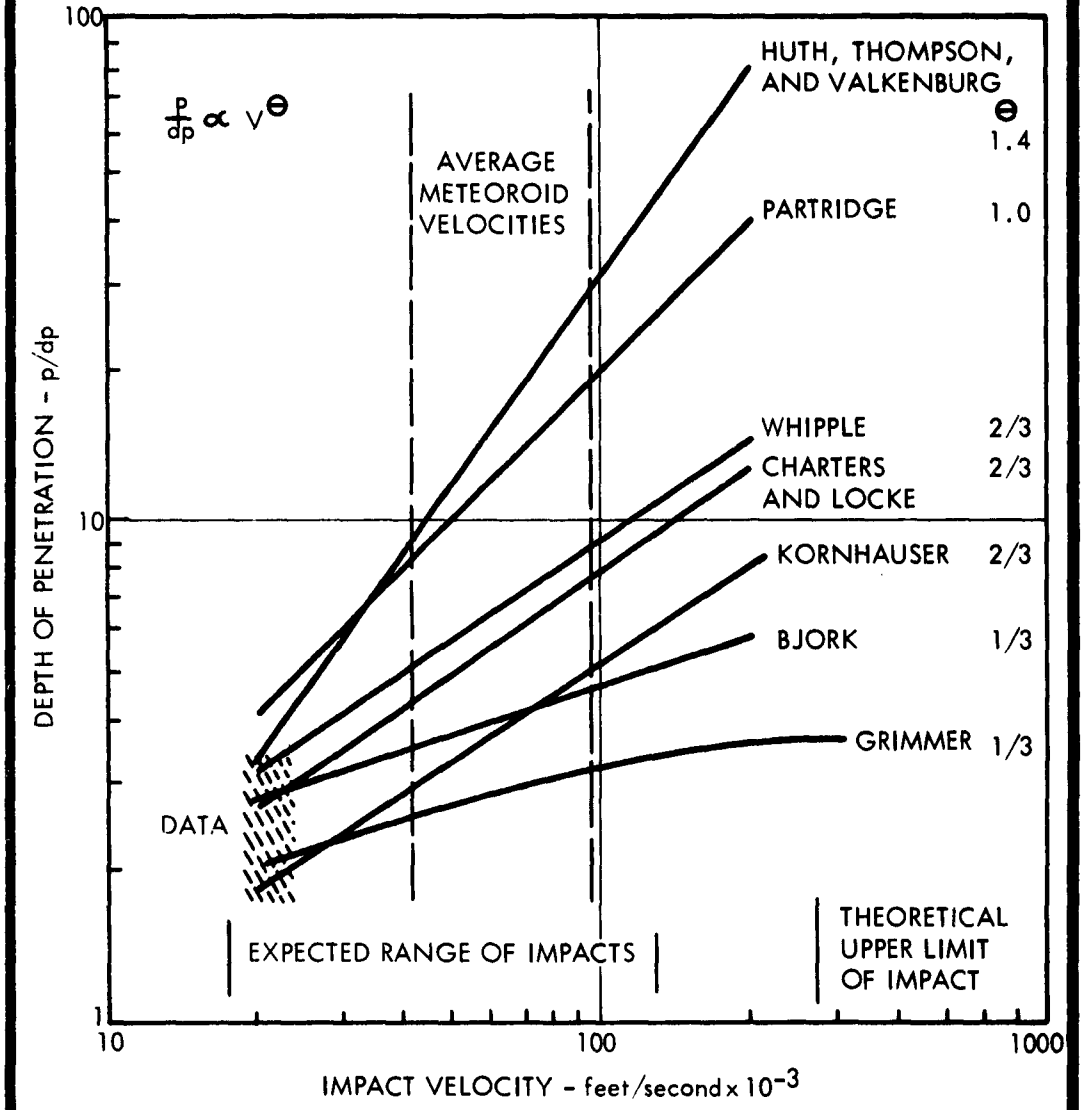

FIGURE A-6. COMPARISON AMONG PENETRATION THEORIES (FROM ARS 2543-62)

17.0-65-2250

5) Spalling - partial blockage of flow passages or short-circuiting of converters by ejection of material on back side of target.

Several protective methods against the meteoroid hazard are theoretically available to the radiator designer: direct armoring (massive or laminated), bumper shields, redundant segmenting, self-sealing systems, and changes of geometry and operating temperature.

1. Direction Armoring

In this approach, a solid mass of material physically stops an impacting particle before it can cause serious damage. This is the approach recommended for thermionic radiators because 1) preliminary design data and and direction calculational methods exist; and 2) circumferential temperature variations can be reduced in planar finned tubes. At the heat fluxes required in thermionic converters, large temperature variations at the periphery of the anode may present operational problems which can be mitigated by increasing the conduction path through the armor.

Laminated armor does not apply to thermionic radiators because of the increased resistance to heat transfer imposed by the laminations; laminated armor usually consists of a thermal insulator between solid sheets.

2. Bumper Shields

In the bumper concept, a relatively thin shield of material separated from the surface to be protected disintegrates an impacting particle and diffuses its energy over a greater area. The total thickness of bumper and primary armor required to stop a given particle has been found to be approximately one-half the thickness for regular armor, although considerable variation has been observed in different experiments. Note that, since the bumper imposes an additional resistance to radiation, the effectiveness of this approach will depend upon an evaluation of the bumper's heat transfer properties as well as its protective characteristics. Bumper thickness is a function of target and projectile material properties and projectile size and velocity as well as separation between bumper and armor. Although lack of data excludes this method from preliminary consideration, it should be reassessed when more information becomes available. In thermionic converters, a cesium gap exists between the cathode and anode. At the required gap and anode thickness,

experimental evidence indicates that the bumper effect is negligible; hence, the unit may be treated as solid armor.

3. Redundant Segmenting

This design consists of a number of panels in parallel, a specified number of which will provide the required protection. Damaged panels are isolated from the system. If the probabilities of survival are high, and if a reliable leak-detection and shutoff system can be developed, redundant segmenting would be a weight saving solution. Further research is necessary to determine whether or not segmenting will increase system reliability.

4. Self-Sealing Systems

Self-sealing demands a minimum amount of armor, since punctures are automatically repaired. However, a satisfactory self-sealing technique remains to be developed.

5. Changes in Geometry and Operating Temperatures

Increased operating temperatures might reduce the vulnerable area, depending on the influence of temperature on efficiency. The desirability of temperature changes can only be determined from extensive system calculations. Optimization of individual tube and overall radiator configuration in terms of system weight would indicate the armor required to minimize total weight.

E. METEOROID CALCULATIONS

1. Derivation of Armor Equations

The cumulate meteoroid flux can be expressed as a function of particle mass by the equation,

$$F_{>} = \alpha\, m^{-\beta} \quad . \tag{1}$$

If $\bar{N}_{>}$ is defined as the average number of impacts on vulnerable area, A, in time, τ, by a critical mass, m_c, then from Equation (1)

$$\bar{N}_{>} = A\tau F_{>} = A\tau\alpha\, m_c^{-\beta} \quad . \tag{2}$$

Assuming that the flux in space is isotropic (actually it is anistropic; to a randomly tumbling vehicle, however, the intergrated flux appears isotopic),

the flux emitted per unit area per unit solid angle obeys Lambert's cosine relation and

$$F_{>} = \int_{\omega} F_{\omega} \cos \lambda \, dw = \pi F_{\omega} \quad , \tag{3}$$

where F_{ω} is the isotropic flux in space. The differential number of critical impacts, $d\bar{N}_{>}$, occuring per unit solid angle per unit projected surface is given by

$$d\bar{N}_{>} = F_{\omega} \tau_A \cos \lambda \, d = \frac{\alpha \, m_c^{-\beta}}{\pi} \tau_A \cos \lambda \, d \quad . \tag{4}$$

A relationship between the critical mass, m_c, and the penetration depth is needed. On the basis of data obtained in currently achievable velocity ranges, the depth of penetration can probably be expressed by

$$P_{\infty} = \gamma \, d \left(\frac{\rho_p}{\rho_T} \right)^{\phi} \left(\frac{\bar{v}_c}{c} \right)^{\theta} \quad . \tag{5}$$

For a spherical projectile, the diameter can be written as

$$d = \left(\frac{6}{\pi} \right)^{1/3} m^{1/3} \, \rho_p^{-1/3} \quad . \tag{6}$$

The required armor thickness in terms of a thin plate and spalling factor "a" and depth of penetration is

$$t = a \, P_{\infty} \quad . \tag{7}$$

The critical damage appears to depend on the impact angle; thus, the velocity governing the damage is

$$\bar{v}_c = \bar{v} \, (\cos \lambda)^n \quad . \tag{8}$$

Combining Equations (5), (6), (7) and (8), and solving for the mass of the penetrating particle,

$$m = \left(\frac{t}{K}\right)^3 \left(\frac{\bar{v}\cos^n\lambda}{c}\right)^{-3\theta} , \tag{9}$$

$$K = \left[a\gamma\left(\frac{6}{\pi}\right)^{1/3} \rho_p^{-1/3} \left(\frac{\rho_p}{\rho_T}\right)^{\phi}\right] . \tag{10}$$

Substituting Equation (10) into (4) gives:

$$d\bar{N}_> = \frac{\alpha}{\pi}\left(\frac{t}{K}\right)^{-3\beta}\left(\frac{\bar{v}}{c}\right)^{3\theta\beta} \tau_A (\cos\lambda)^{3n\theta\beta+1} d_\omega . \tag{11}$$

By converting Equation (11) to spherical coordinates and integrating over half space, the final expression for the critical number of impacts can be derived:

$$\bar{N}_> = \frac{\alpha}{\pi}\left(\frac{t}{K}\right)^{-3\beta}\left(\frac{\bar{v}}{c}\right)^{3\theta\beta}\tau_A \int_0^{2\pi} d\psi \int_0^{\pi/2} (\cos\lambda)^{3n\theta\beta+1} \sin\lambda d\lambda$$

$$= \alpha\tau_A\left(\frac{t}{K}\right)^{-3\beta}\left(\frac{\bar{v}}{c}\right)^{3\theta\beta}\left[\frac{2}{3n\theta\beta+2}\right] . \tag{12}$$

Because of the random nature of the events, the meteoroid punctures may be expected to follow a Poisson distribution, given by

$$P(n) = \frac{(\bar{N}_>)^n e^{-\bar{N}_>}}{n!} . \tag{13}$$

The probability that no puncture will occur is calculated from Equation (13) by setting n = o:

$$P(o) = e^{-\bar{N}_>} . \tag{14}$$

Solving for $\bar{N}_>$ from Equation (14) gives

$$\bar{N}_> = -\ln P(o). \tag{15}$$

Combining Equations (15) and (12) and solving for t gives the final expression for the armor thickness:

$$t = K\left[\frac{\alpha \tau_A}{-\ln P(o)}\right]^{1/3\beta}\left(\frac{\bar{v}}{c}\right)^{\theta}\left[\frac{2}{3n\theta\beta + 2}\right]^{1/3\beta}$$

$$= \left[a\gamma\left(\frac{6}{\pi}\right)^{1/3}\rho_p^{-1/3}\left(\frac{\rho_p}{\rho_T}\right)^{\phi}\right]\left[\frac{\alpha \tau_A}{-\ln P(o)}\right]^{1/3\beta}\left(\frac{\bar{v}}{c}\right)^{\theta}\left[\frac{2}{3n\theta\beta + 2}\right]^{1/3\beta} \quad (16)$$

The nomenclature and constants of Equation (16), based on the latest theoretical and experimental studies, are listed below.

t = required armor thickness in cm

a = finite plate and spalling factor = 1.75

γ = constant in penetration correlation = 2

ρ_p = mean meteoroid particle density = 0.6 gm/cc

ρ_T = armor material density - gm/cc

α = constant in flux distribution = 1.01×10^{-10}

β = exponent in flux distribution = 1.34

A = external armor surface - ft^2

$P(o)$ = design probability for no critical damage to radiator system

τ = mission time - days

$\bar{v}$ = average meteoroid velocity = 30 km/sec

c = sonic velocity of the armor material - km/sec = $2.63 \times 10^{-3} \frac{E_t}{T}$

where E_t = Young's modulus at operating temperature - lb/in^2.

ϕ = exponent in penetration correlation = 1/2

θ = exponent in penetration correlation = 2/3

n = exponent for velocity impact angle dependence = 1

Substituting the constants and simplifying Equation (16) yields:

$$t = \left[1.75 \times 2 \left(\frac{6}{\pi}\right)^{1/3} (0.6)^{-1/3} \left(\frac{0.6}{\rho_T}\right)^{0.5}\right]\left[\frac{1.01 \times 10^{-10} \tau_A}{-\ln P(o)}\right]^{\frac{1}{3 \times 1.34}}$$

$$\times \left(\frac{30}{2.63 \times 10^{-3}\sqrt{E_t/\rho_T}}\right)^{0.667}\left[\frac{2}{2 \times 1 \times 0.667 \times 1.34 \times 2}\right]^{\frac{1}{3 \times 1.34}}$$

$$= \left[\frac{4.00}{\sqrt{\rho_T}}\right]\left[\frac{1.01 \times 10^{-10} \tau_A}{\ln P(o)}\right]^{0.249} \times 500 \left(\sqrt{\frac{\rho_T}{E_T}}\right)^{0.667} \times 0.853$$

$$= 5.5 \left[\frac{\tau_A}{-\ln P(o)}\right]^{0.249} \frac{1}{E_t^{0.334}\, \rho_T^{0.166}} . \qquad (17)$$

A refinement of the calculations to include the fact that a variable thickness of actual armor material may be used in thermionic radiators because of initial differences in component thickness (which are part of the total armor) will now be derived. For m portions having areas, A_i, and equivalent thicknesses, t_i, the joint probability is:

$$P(o) = \prod_{i=1}^{m} e^{-\bar{N}_{>i}} . \qquad (18)$$

After taking the logarithm of Equation (18), the joint probability becomes

$$-\ln P(o) = \sum_{i=1}^{m} \bar{N}_{>i} . \qquad (19)$$

Combining Equations (12) and (19) yields the final expression for the variable armored case:

$$-\ln P(o) = \alpha\tau\left[\frac{2}{3n\theta\beta + 2}\right] \sum_{i=1}^{m} A_i \left(\frac{t}{K}\right)_i^{-3\beta} \left(\frac{\bar{v}}{c}\right)_i^{3\theta\beta} . \qquad (20)$$

2. Geometry Calculations

Assume that the radiator can be divided into a number of modules having the following configuration.

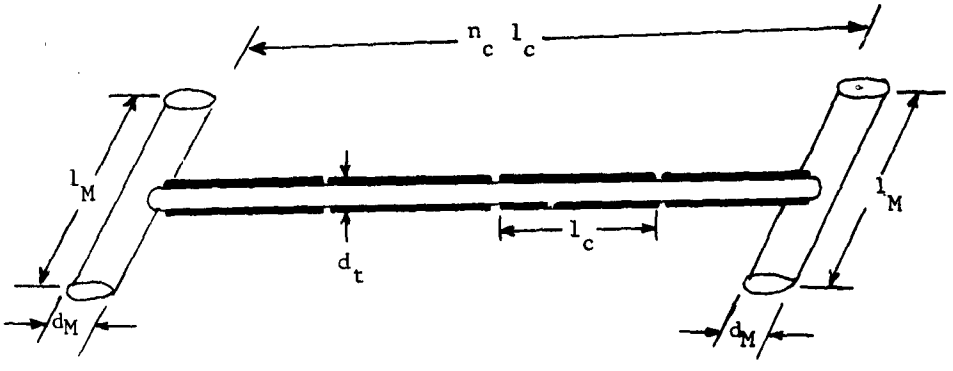

The vulnerable or outside surface area can be expressed as:

$$A = \left\{ N\ 2\left[\pi(d_M + 2\ t_M)\ l_M\right] + n_c\left[\pi(d_T + 2\ t_c)\ l_c\right]\right\}$$

$$= N\left\{(2\pi d_M\ l_M + n\pi d_t\ l_c) + 2\pi(2\ l_M\ t_M + n\ l_c\ t_c)\right\}$$

$$= N\left\{A_{\substack{\text{total inside surface}\\ \text{exposed to fluid}}} + t_M\ (2\pi L_{\text{total length of manifolds}})\right.$$

$$\left. + t_t\ (2\pi L_{\text{total length of converter carrying tubes}})\right\}, \quad (21)$$

where t_t is the sum of the tube, converter, and armor thicknesses (where applicable). That the tube and converter supply some protection from the meteoroids must be accounted for in the armor calculations be in the following manner. In the derivation of Equation (17), it was found that the armoring effect of materials varied as

$$t \propto \frac{1}{E_t^{0.334}\ \rho_T^{0.166}} \quad . \tag{22}$$

Since the various component materials in series resist penetration, the effective protection of these materials, in terms of equivalent thickness of the armoring material, may be expressed as:

$$t_{equiv} = \left(\frac{E_{tube}}{E_{armor}}\right)^{0.334} \left(\frac{\rho_{tube}}{\rho_{armor}}\right)^{0.166} t_{tube} + \left(\frac{E_{conv}}{E_{armor}}\right)^{0.334} \left(\frac{\rho_{conv}}{\rho_{armor}}\right)^{0.166} t_{converter} + t_{\substack{external \\ armor.}} \tag{23}$$

To determine the required armor thickness without resorting to the variable armor equation (20), it must be assumed that $t_c = t_M$; i.e., that the bare manifold and converter thicknesses are the same. This approximation is probably realistic, since a relatively thick manifold will be required for structural rigidity. Using this assumption, Equation (21) simplifies to:

$$A = N_{modules} \left\{ A_{inside\ surface} + t\ (2\pi L_{tubes + Manifolds}) \right\}. \tag{24}$$

Equations (17), (23), and (24) can now be combined to yield an expression for the required armor thickness as a function of materials, probability of non-puncture, mission time, number of modules and inside surface area, and developed length of each module:

$$t = \left[\frac{5.5}{E_a^{0.334}\ \rho_A^{0.166}}\right]\left[\frac{\tau}{-\ln P(o)}\right]^{0.249}\left[N\left(A_i + 2\pi L \frac{t_{equiv}}{30.48}\right)\right]^{0.249} \tag{25}$$

BIBLIOGRAPHY

1. J. Loeffler, et al., "Meteoroid Protection for Space Radiators," Paper No. 2543-62, ARS Space Power Systems Conf., September 1962.

2. J. R. Davidson, et al., Environmental Problems of Space Flight Structures - Meteoroid Hazard, NASA-TN-D1493.

3. J. O. Funkhouser, A Preliminary Investigation of the Effect of Bumpers as a Means of Reducing Projectile Penetration, NASA-TN-D-802.

4. W. H. Kinard, et al, An Investigation of High-Velocity Impact Cratering into Non-Metallic Targets and Correlation of Penetration Data for Metallic and Non-Metallic Targets, NASA-TN-D-726.

5. Aerojet-General Corporation, Impact and Penetration of 0.100 inch Aluminum Plates by Aluminum Projectiles at 29,000 to 33,000 ft/sec, APGC-TDR-62-40.

6. Fourth Symposium on Hypervelocity Impact - April 1960, APGC-TR-60-39, (Vol. II and III).

7. Fifth Symposium on Hypervelocity Impact - Denver Colorado, October 1961, Vol. 1, Parts 1 and 2.

8. General Electric Co., Theory of High Speed Impact, March 1962, APGC-TDR-62-20.

DISTRIBUTION LIST

Cys	ACTIVITIES AT WPAFB
1	ASAPT
1	ASAPR
1	ASRMFP
3	ASRMFP-2 (Capt. Redden)
1	ASRNET

OTHER DEPT OF DEFENSE ACTIVITIES

Navy

1 Office of Naval Research
Code 429
ATTN: Lt. Cmdr. John J. Connelly
Washington 25, D. C.

Air Force

1 AFCRL (CRZAP)
ATTN: Mr. A. W. Diniak
L. G. Hanscom Field
Bedford, Massachussetts

1 AFOSR (SRHPM)
ATTN: Dr. Milton Slawsky
Bldg. T-D
Washington 25, D. C.

1 SSD (SSTRE, Capt. W. Hoover)
AF Unit Post Office
Los Angeles 45, California

22 ASTIA (TIPDR
Arlington Hall Stn
Arlington 12, Virginia

Cys	OTHER U.S. GOVT. AGENCIES
1	U.S. Atomic Energy Commission Division of Reactor Development ATTN: Cmdr. W. Schoenfeld Washington 25, D. C.
1	Advanced Research Projects Agency ATTN: Dr. John Huth Washington 25, D. C.
1	Jet Propulsion Laboratory Spacecraft Secondary Power Section ATTN: Mr. Paul Goldsmith 4800 Oak Park Drive Pasadena, California
1	Aerospace Corporation ATTN: Library Technical Document Group Post Office Box 95085 Los Angeles 45, California
1	NASA - Lewis Research Center ATTN: Mr. Roland Breitweiser 210000 Brookpark Road Cleveland 35, Ohio

OTHERS

1	Hughes Research Laboratories ATTN: Dr. Roland Knechtli Malibu, California
1	Babcock and Wilcox Company ATTN: Mr. P. F. Schutt P. O. Box 1260 Lynchburg, Virginia
1	Radio Corporation of America ATTN: Mr. F. G. Block Electronic Tube Division Lancaster, Pennsylvania